ACS Macro Letters

Letter

pubs.acs.org/macroletters

Harnessing Anisotropic Nanoposts to Enhance Long-Range Orientation Order of Directed Self-Assembly Nanostructures via Large Cell Simulations

Liangshun Zhang,* Liquan Wang, and Jiaping Lin*

Shanghai Key Laboratory of Advanced Polymeric Materials, State Key Laboratory of Bioreactor Engineering, Key Laboratory for Ultrafine Materials of Ministry of Education, School of Materials Science and Engineering, East China University of Science and Technology, Shanghai 200237, China

Supporting Information

ABSTRACT: Self-assembly behaviors of cylinder-forming diblock copolymers directed by an array of anisotropic nanoposts with elliptical shape are explored by large cell simulations of self-consistent field theory. The strategy using elliptical nanoposts allows us to generate long-range order cylinders with single orientation by suppressing other selections of cylinder alignment. The anisotropy of nanoposts plays a significant role in improving the tolerance of commensurability conditions between the dimensions of nanopost lattices and the period of cylinders. Moreover, the local defect structures could be regulated through varying the spacing and orientation of elliptical nanoposts. This work may provide useful guidelines for designing the topographical templates and lay the groundwork for fabricating well-ordered nanostructures of block copolymer lithography.

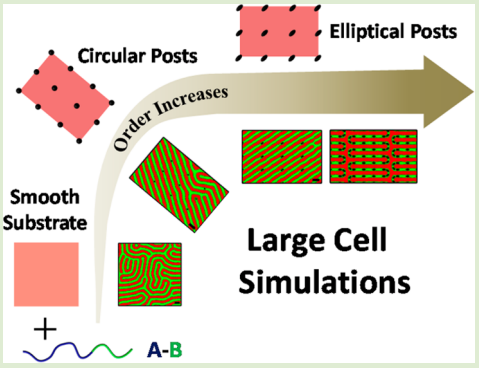

For the last several decades, self-assembly of block copolymers has been extensively studied for its potential utility in emerging nanotechnologies involving nanolithography, nanotemplating, and ultra-high-density storage media.[1−4] However, the structures formed during spontaneous self-assembly commonly contain many defects that limit their technological applications. Directed self-assembly of block copolymers in thin films was recently demonstrated to form defect-free nanostructures over large areas and precisely register the domains on the substrates.[5−11]

One of the most investigated techniques of directed self-assembly is graphoepitaxy.[12−21] In experiments, Ross and co-workers designed a rectangular array of chemically functionalized topographical nanoposts to direct the self-assembly of cylinder-forming polystyrene-*block*-polydimethylsiloxane (PS-*b*-PDMS) diblock copolymers on the substrates.[16] The in-plane orientation and order of the cylinders are controlled by the commensurability conditions between the dimensions of rectangular lattice of posts and natural period of PDMS cylinders. In most cases, large area-order cylinders are formed by choosing appropriate spacing of circular nanoposts. As the nanopost spacing increases, there is a tendency to form a 'polycrystalline' structure with several orientations. Such observations of directed self-assembly are also confirmed by computer simulaitons.[16,18] This poses a significant stumbling block to achieve the long-range order patterns due to the isotropic characteristic of circular nanoposts used in experiments.

A further challenge in the template design for block copolymer lithography is to find a set of features that would provide additional orientation guidance to suppress other selections of cylinder alignment. Sparked by recent works of Chang et al.,[22,23] we theoretically design an array of anisotropic nanoposts with elliptical shape to direct the self-assembly of block copolymers via self-consistent field theory (SCFT) of inhomogeneous polymeric fluids.[24−26] The elliptical nanoposts have the ability to exclusively guide the orientation to achieve the well-aligned nanostructures. Figure 1 displays the schematic illustration of model for the self-assembly of block copolymers directed by the elliptical nanoposts. The AB diblock copolymer melts are confined between the substrate and air−polymer interface. The volume fraction of the B blocks is fixed as f_B = 0.32. Since solvent uptake reduces the effective interaction parameter and the coarse-graining segment is larger than the chemical repeat unit,[27] the combined Flory−Huggins parameter between the A and B segments is chosen as χN = 15.0, which is much lower than the bulk value. The air−polymer interfaces, substrates, and nanoposts attract the B blocks of copolymers.

To explore order degree of patterns and orientation distribution of block copolymer cylinders, which cannot be obtained from the unit cell calculations, a series of large cell SCFT simulations via acceleration of graphics-processing units are performed. In the SCFT calculations, the block copolymers self-assemble into the B-rich cylinders with period $L_0 \sim 3.5R_g$ in

Received: May 31, 2014
Accepted: July 9, 2014
Published: July 11, 2014

   dx.doi.org/10.1021/mz5003257 | ACS Macro Lett. 2014, 3, 712−716

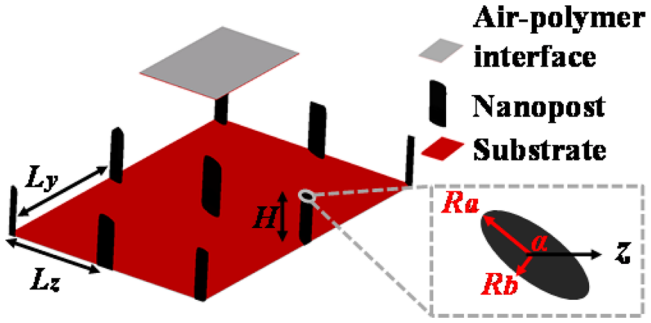

Figure 1. Schematic illustration of template consisting of an array of elliptical nanoposts (black) between air−polymer interface (gray) and substrate (red). The spacing of nanoposts in the y and z directions is denoted by L_y and L_z, respectively. H represents the height of nanoposts. Inset is the top view of the elliptical nanopost with long axis R_a, short axis R_b, and orientation angle α between the long axis and z direction.

the bulks, where R_g is the unperturbed gyration radius of polymer chains. Due to the features of the B-wetting substrate and air−polymer interface, the film thickness is set as $2.2L_0$ to ensure the formation of cylinder monolayer. The Dirichlet boundary conditions are applied in the normal (x) direction. The periodic boundary conditions are imposed to the lateral (y and z) directions in an $\sim 21.0L_0 \times 21.0L_0$ simulation cell. We could estimate the real size of the simulation cell by relating the period L_0 to that of some experimental data. For example, the samples of PS-*b*-PDMS with f_{PDMS} = 33.5% and total molecular weight of 45.5 kg·mol^{-1} self-assemble into cylinder structures with period ~35 nm.[16] The actual size of the cell is about 0.74 × 0.74 μm^2 in the lateral directions. More details about the model and numerical method are presented in the Supporting Information (SI).

After obtaining the patterns of directed self-assembly, we develop another computer program to calculate in-plane orientation distribution of cylinders and order parameter of patterns. The interfaces between the A- and B-rich domains and the local tangent vectors along the interfaces are obtained from the averaging density field in the y−z plane. The angle between the tangent vector and z-axis is denoted by θ, which is illustrated in the inset of Figure 2a. The distribution of angle θ is used to characterize the local orientation distribution of cylinders. To quantitatively measure the order of patterns on the substrates, we introduce order parameter S to describe the order degree of cylinder alignment, which is defined as[28,29]

$$S = \frac{1}{2}\langle 3\cos^2\vartheta - 1\rangle \quad (1)$$

Here, ϑ is the angle between the tangent vector of interface and the local director. As the order parameter S approaches one, perfectly ordered cylinders are generated in the template.

For the sake of comparison, Figure 2a shows the top-view pattern of cylinder-forming block copolymers self-assembling on the smooth substrates. The monolayer morphology of B-rich cylinders exhibits only short-range order. This fact is clearly demonstrated by the approximately uniform distribution of cylinder orientation (lower panel of Figure 2a).

To impose long-range order on the cylinder structures, a rectangular array of circular nanoposts is exploited to direct the self-assembly of block copolymers on the substrates. The patterns templated by the circular nanoposts with height H = $1.1L_0$ and spacing at L_z/L_0 = 2.1, 3.6, and 4.0 are displayed in

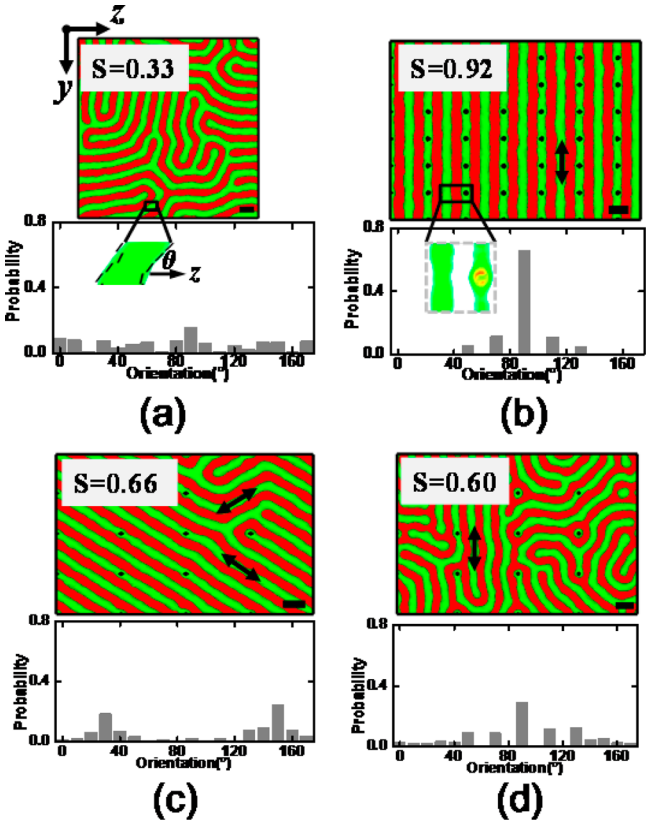

Figure 2. Patterns (upper panels) and local orientation distributions (lower panels) of cylinder monolayers of block copolymers in templates. (a) Untemplated monolayer of cylinders on a smooth substrate. (b−d) Monolayer of cylinders registered by circular nanoposts with height H = $1.1L_0$ and L_z/L_y = 1.5. The spacing L_z/L_0 increases from (b) 2.1 to (c) 3.6 and (d) 4.0. The red and green colors represent the substrate and B-rich cylinders, respectively. The black domains represent the nanopost positions on the substrate. The scale bars indicate the period L_0 of cylinders formed in the bulks. The black arrows represent the commensurability orientation of cylinders. Note that only a 1/4 portion of monolayers are displayed and the air−polymer interfaces and B-rich domains close to the substrates are not drawn in the top-view of the pattern. The local orientations θ of cylinders, which are schemed in the inset of (a), are characterized by the angles of tangent vectors at the interfaces with respect to the z-axis. Inset of (b) shows the enlarged profile of local density distribution of B-type segment around a nanopost.

Figures 2b−d, respectively. The three-dimensional view of patterns is also presented (Figure S3 of SI). For the case of L_z/L_0 = 2.1, the period of cylinders is commensurate with the spacing L_z of nanoposts. The B-rich cylinders contact the nanoposts to reduce the interfacial energy and orient along the y-axis to minimize the strain energy. Due to a small amount of necking or undulation near the nanoposts as illustrated in the inset of Figure 2b, there also exist some local orientations deviated from the y direction. The main reason is that the nanoposts lead to distortion of polymer chains surrounding them. The order parameter S of the pattern has a value of 0.92, indicating that the cylinders of block copolymers are perfectly registered on the substrates by the circular nanoposts.

However, as the spacing of nanoposts increases, the commensurate nanoposts are not very effective in directing the self-assembly of block copolymers. As predicted from the commensurability condition,[16] the cylinders of block copolymers are expected to align diagonally with respect to the

dx.doi.org/10.1021/mz5003257 | ACS Macro Lett. 2014, 3, 712−716

nanopost lattice when the spacing L_z/L_0 of nanoposts has a value of 3.6. However, there is no single cylinder orientation that is completely filled in the template (Figure 2c). The orientation distribution with two peaks at θ = 30° and 150° implies that two possible orientations of cylinders appear and "polycrystalline" nanostructures with grain boundaries are produced in the pattern. For the case of L_z/L_0 = 4.0, the cylinders are expected to orient along the y-axis. However, the simulations produce cylinders with both the commensurability and strained orientations, as depicted in Figure 2d. It is also found that some cylinders are not connected to the nanoposts even though the posts have a layer of B blocks surrounding them. These facts lead to a broad distribution of cylinder orientation and a poor order of cylinder alignment. It should be mentioned that the film thickness and post height also have effects on the order structures of block copolymers.[17,22] As the posts are too short or tall, the B-rich cylinders are not aligned in a preferential orientation. Film thickness affects mainly on the number of cylinder layers. Increasing the film thickness leads to the formation of cylinder multilayers.

As illustrated above, when the spacing of nanoposts satisfies the commensurability condition of cylinder period, the block copolymers could be directed into large-area patterns with long-range order. However, due to the isotropic characteristic of circular nanoposts, the cylinders with degenerate orientations or mixture of commensurability and strained orientations are observed for the case of large spacing of nanoposts. These computational findings are consistent with the experimental results of Ross and co-workers.[16,22] To introduce the orientation selection of cylinders in the template, the nanoposts with circular symmetry could be replaced by the well-spaced elliptical nanoposts, which open a new route to deterministically guide the in-plane orientation of cylinder monolayers.

Figure 3 shows the self-assembly behaviors of block copolymers directed by the elliptical nanoposts with a range of aspect ratio R_a/R_b. The monolayer patterns of cylinders registered by an array of elliptical nanoposts with aspect ratio R_a/R_b = 1.6 and 3.0 are depicted in Figure 3a and b, respectively. As the nanoposts have the anisotropic characteristic, the probability of commensurability orientation (90°) in the patterns has an increase in comparison with the case of the circular nanoposts (Figure 2d), suggesting that a preference of cylinder orientation could be established by the anisotropic nanoposts (Figure 3a). Nevertheless, there still exist some cylinders oriented along the unwanted directions. When the anisotropy of nanoposts further increases, the block copolymers are forced to align parallel to the long axis of nanoposts, and thereby a long-range orientation order pattern is achieved in the template (Figure 3b).

To estimate the anisotropic effects of nanoposts on the order of patterns, the order parameters defined in eq 1 are calculated. As shown in Figure 3c, the circular nanoposts (case of R_a/R_b = 1.0) produce the patterns with poor order. As the nanoposts become anisotropic, the domains around the posts are strongly distorted. This results in an increase of stretching of polymer chains or entropic energy penalty of system. To alleviate the effects, the polymer domains are forced to orient along the long axis of elliptical nanoposts. As a result, an increase of the aspect ratio leads to the enhancement of alignment order of cylinders. When the aspect ratio of nanoposts has a value of 2.4, the cylinders are directed along the expected commensurate orientation. The order parameter of such pattern approaches one. As the anisotropy of nanoposts further increases, the

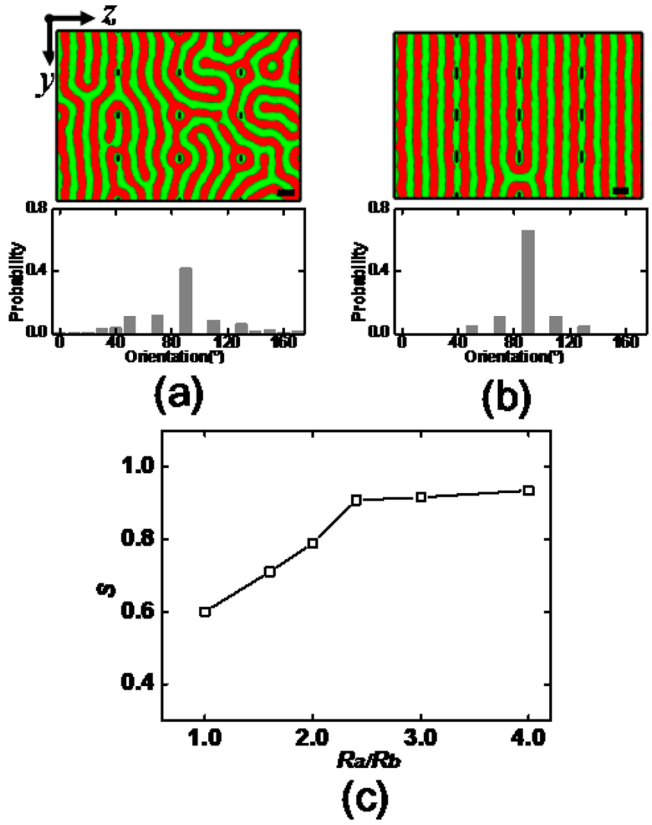

Figure 3. Patterns (upper panels) and local orientation distributions (lower panels) of cylinder monolayers programmed by elliptical nanoposts with different aspect ratios (a) R_a/R_b = 1.6 and (b) R_a/R_b = 3.0 at fixed parameters L_z/L_y = 1.5 and L_z/L_0 = 4.0. The elliptical nanoposts orient along the y-axis. Note that only a 1/4 portion of patterns are shown. (c) Order parameter S of pattern as a function of aspect ratio R_a/R_b.

cylinders are still perfectly registered on the substrates and the order parameter remains a high value. Recently, Xie et al. exploited anisotropic posts to produce large-scale order patterns from the directed self-assembly of block copolymers.[21] The anisotropic posts in the Xie's idea are used to control the orientation of the nucleus, whereas the elliptical posts are introduced to suppress other cylinder orientations by reducing the entropic penalty in our scheme.

It is important to note that the number of registered cylinders on the substrates is highly enhanced by the elliptical nanoposts. As shown in Figure 3 and Figure S4 of SI, the number of B-rich cylinders between the nanoposts in the z direction increases correspondingly with the spacing L_z, and the maximum value of cylinder number could reach 5 without losing the long-range order. This is a significant improvement compared with the case of circular nanoposts, where the dense array of nanoposts is necessitated to produce well-aligned nanostructures. This conclusion means that the orientation guidance by the sparse array of elliptical nanoposts can be considered to further enhance the throughput of electron-beam lithography system, which will dramatically decrease the electron-beam writing times and lower the fabrication cost of semiconductor devices.

Another important aspect of template design is the tolerance of commensurability condition for the nanoposts, which will lower the precision requirements in the template fabrication process. To clarify the tolerance for the nanoposts with

dx.doi.org/10.1021/mz5003257 | ACS Macro Lett. 2014, 3, 712−716

different shapes, we consider the case of elliptical nanoposts oriented at 33.7° commensurability angle and vary the spacing of nanoposts. As shown in Figure 4a, the cylinders are not

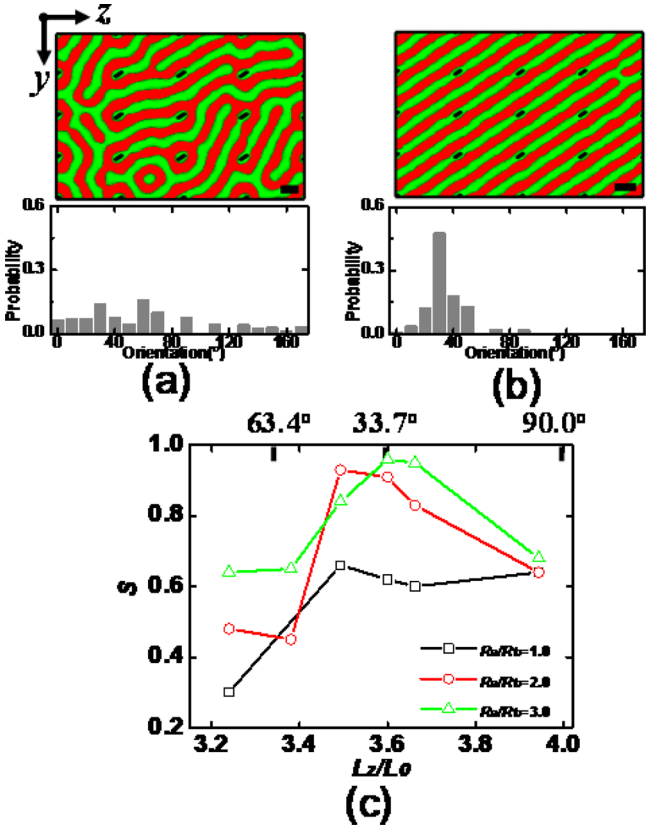

Figure 4. Patterns (upper panels) and local orientation distributions (lower panels) of cylinder monolayers guided by elliptical nanoposts with different values of spacing (a) L_z/L_0 = 3.43 and (b) L_z/L_0 = 3.50. The aspect ratio R_a/R_b and orientation angle α of elliptical nanoposts are 2.0 and 33.7°, respectively. Note that only a 1/4 portion of patterns are shown. (c) Order parameter S of pattern as a function of spacing L_z/L_0 of nanoposts under various aspect ratios R_a/R_b. The angles shown on the top axis indicate the commensurability angle at the corresponding spacing of circular posts.

aligned parallel to the long axis when templated by the elliptical nanoposts with spacing L_z/L_0 = 3.43, which has a large deviation from the commensurability spacing L_z/L_0 = 3.60. From the orientation distribution, it is also found that several orientations 33.7° and 63.4° of cylinders coexist in the pattern. When the spacing of elliptical nanoposts is slightly deviated from the optimum spacing, the cylinders preferentially align parallel to the long axis of elliptical nanoposts, which is illustrated in Figure 4b.

Figure 4c shows the order parameter S of pattern as a function of the spacing L_z/L_0 of elliptical nanoposts with various values of aspect ratio R_a/R_b. The circular nanoposts, corresponding to the case of R_a/R_b = 1.0, cannot effectively program the cylinders to form long-range order patterns due to lacking orientation selection. As the nanoposts become anisotropic, the cylinders are encouraged to align parallel to the long axis of elliptical nanoposts. However, as the spacing is largely deviated from the commensurability spacing L_z/L_0 = 3.60, the posts lead to considerable distortion of domains. The B block-nanopost interfacial energy cannot make up the loss of chain entropy. This gives rise to the coexistence of multiple orientations and breakdown of long-range orientation order. When the deviation is small, for example, in the range of spacing 3.50 ≤ L_z/L_0 ≤ 3.66, the strained orientations are frustrated by the elliptical posts, and the cylinders with 33.7° orientation occupy the entire substrates. Such findings provide significant guidance for experimentalists to lower the precision requirement of template design by choosing the anisotropic nanoposts.

In addition to program the periodic structures of block copolymer cylinders on the entire substrates, one could locally control the orientation of cylinders to form nontrivial structures such as zigzag, T-junction, and nested-elbow structures (Figure S5 of SI), which are very similar to the structures registered by the circular nanoposts.[16,17] On the other hand, replacing the circular nanoposts with elliptical motifs also gives rise to the local change of complex nonperiodic structures. For instance, by placing additional nanoposts at bends, the cylinders are reoriented and folded into tight meander structures shown in Figures 5a,b. Although two types of nanoposts have the ability

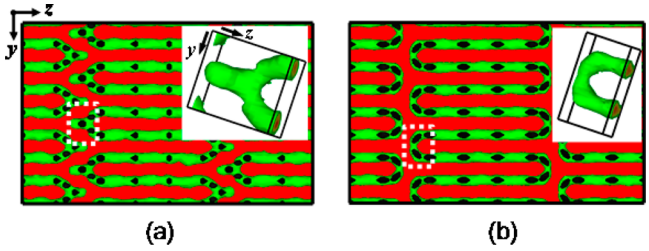

Figure 5. Meander structures with sharp bends by adding a group of nanoposts with (a) circular and (b) elliptical shapes at strategic locations. Insets are the three-dimensional enlarged view of local density distribution of B-type segments enclosed in the dashed boxes.

to produce the meander structures by the template design, the local defects emerge as a significant difference. For the case of circular nanoposts, a complex omega shape with a protrusion is formed (inset of Figure 5a). Although the omega shape are not seen in the block copolymer lithography so far, they were observed in the Gido et al. work about the kink grain boundaries of block copolymers.[30] The formation of omega shape results from a huge reduction in the curvature energy of domains,[31] which is enough to compensate for the increase in the interfacial area and packing frustration due to the large protrusions of defects. Introducing elliptical nanoposts into the template could relieve such effects at the sharp bends, and trigger the transition from the protrusion omega shape to a smooth "chevron" shape (inset of Figure 5b). These observations manifest the fact that the optimized template containing the elliptical nanoposts is able to reduce the roughness of complex nanostructures.

In summary, we first report the graphics-processing unit implementation of polymer field-theoretic simulations for the directed self-assembly of block copolymers. The large cell simulations enable us to analyze orientation distribution of cylinders and order degree of patterns. Using the simulations, we corroborate the results that the long-range order nanostructures with single orientation are achieved by virtue of the anisotropic nanoposts. A large incommensurability is tolerated without breaking the long-range orientation order for the case of anisotropic nanoposts. Additionally, the anisotropic nanoposts give rise to the local change of complex patterns with nonperiodic features. The preceding results would provide

dx.doi.org/10.1021/mz5003257 | ACS Macro Lett. 2014, 3, 712−716

useful information to rationally design the topographical template containing anisotropic motifs to achieve long-range orientation order nanostructures.

■ ASSOCIATED CONTENT

Supporting Information

Part A: Model of directed self-assembly of diblock copolymers; Part B: Numerical method; Part C: Three-dimensional view of directed self-assembly patterns; Part D: Patterns of cylinders registered by a sparse array of elliptical nanoposts; Part E: Complex nanostructures registered by elliptical nanoposts. This material is available free of charge via the Internet at http://pubs.acs.org.

■ AUTHOR INFORMATION

Corresponding Authors

*E-mail: zhangls@ecust.edu.cn.
*E-mail: jlin@ecust.edu.cn.

Notes

The authors declare no competing financial interest.

■ ACKNOWLEDGMENTS

This work was supported by the National Natural Science Foundation of China (51203049, 21234002) and Research Fund for the Doctoral Program of Higher Education of China (20120074120003).

■ REFERENCES

(1) Chai, J.; Buriak, J. M. *ACS Nano* **2008**, *2*, 489−501.
(2) Zschech, D.; Kim, D. H.; Milenin, A. P.; Scholz, R.; Hillebrand, R.; Hawker, C. J.; Russell, T. P.; Steinhart, M.; Gösele, U. *Nano Lett.* **2007**, *7*, 1516−1520.
(3) Naito, K.; Hieda, H.; Sakurai, M.; Kamata, Y.; Asakawa, K. *IEEE Trans. Magn.* **2002**, *38*, 1949−1951.
(4) International Technology Roadmap for Semiconductors, 2007; http://www.itrs.net.
(5) Segalman, R. A. *Mater. Sci. Eng., R* **2005**, *48*, 191−226.
(6) Stoykovich, M. P.; Müller, M.; Kim, S. O.; Solak, H. H.; Edwards, E. W.; de Pablo, J. J.; Nealey, P. F. *Science* **2005**, *308*, 1442−1446.
(7) Ruiz, R.; Kang, H.; Detcheverry, F. A.; Dobisz, E.; Kercher, D. S.; Albrecht, T. R.; de Pablo, J. J.; Nealey, P. F. *Science* **2008**, *321*, 936−939.
(8) Koo, K.; Ahn, H.; Kim, S.-W.; Ryu, D. Y.; Russel, T. P. *Soft Matter* **2013**, *9*, 9059−9071.
(9) Hardy, C. G.; Tang, C. *J. Polym. Sci., Part B: Polym. Phys.* **2013**, *51*, 2−15.
(10) Luo, M.; Epps, T. H., III *Macromolecules* **2013**, *46*, 7567−7579.
(11) Bates, C. M.; Maher, M. J.; Janes, D. W.; Ellison, C. J.; Willson, C. G. *Macromolecules* **2014**, *47*, 2−12.
(12) Segalman, R. A.; Yokoyama, H.; Kramer, E. J. *Adv. Mater.* **2001**, *13*, 1152−1155.
(13) Sundrani, D.; Darling, S. B.; Sibener, S. *Nano Lett.* **2004**, *4*, 273−276.
(14) Chai, J.; Wang, D.; Fan, X.; Buriak, J. M. *Nat. Nanotechnol.* **2007**, *2*, 500−506.
(15) Bita, I.; Yang, J. K. W.; Jung, Y. S.; Ross, C. A.; Thomas, E. L.; Berggren, K. K. *Science* **2008**, *321*, 939−943.
(16) Yang, J. K. W; Jun, Y. S.; Chang, J.-B.; Mickiweicz, R. A.; Alexander-Katz, A.; Ross, C. A.; Berggren, K. K. *Nat. Nanotechnol.* **2010**, *5*, 256−260.
(17) Tavakkoli, K. G. A.; Gotrik, K. W.; Hannon, A. F.; Alexander-Katz, A.; Ross, C. A.; Berggren, K. K. *Science* **2012**, *336*, 1294−1298.
(18) Mickiewicz, R. A.; Yang, J. K. W.; Hannon, A. F.; Jung, Y.-S.; Alexander-Katz, A.; Berggren, K. K.; Ross, C. A. *Macromolecules* **2010**, *43*, 8290−8295.
(19) Hannon, A. F.; Ding, Y.; Bai, W.; Ross, C. A.; Alexander-Katz, A. *Nano Lett.* **2014**, *14*, 318−325.
(20) Tang, Q.; Ma, Y. *Soft Matter* **2010**, *6*, 4460−4465.
(21) Xie, N.; Li, W.; Qiu, F.; Shi, A.-C. *Soft Matter* **2013**, *9*, 536−542.
(22) Chang, J.-B; Son, J. G.; Hannon, A. F.; Alexander-Katz, A.; Ross, C. A.; Berggren, K. K. *ACS Nano* **2012**, *6*, 2071−2077.
(23) Chang, J.-B.; Choi, H. K.; Hannon, A. F.; Alexander-Katz, A.; Ross, C. A.; Berggren, K. K. *Nat. Commun.* **2014**, *5*, 3305−3315.
(24) Fredrickson, G. H. *The Equilibrium Theory of Inhomogeneous Polymers*; Oxford University Press: New York, 2006.
(25) Zhang, L.; Sevink, A.; Schmid, F. *Macromolecules* **2011**, *44*, 9434−9447.
(26) Zhang, L.; Lin, J. *Macromolecules* **2009**, *42*, 1410−1414.
(27) Helfand, E.; Tagami, Y. *J. Chem. Phys.* **1972**, *56*, 3592−3601.
(28) de Gennes, P. G.; Prost, J. *The Physics of Liquid Crystals*, 2nd ed.; Oxford University Press: Oxford, U.K., 1993.
(29) Welander, A. M.; Craig, G. S. W.; Tada, Y.; Yoshida, H.; Nealey, P. F. *Macromolecules* **2013**, *46*, 3915−3921.
(30) Gido, S. P.; Thomas, E. L. *Macromolecules* **1994**, *27*, 6137−6144.
(31) Matsen, M. W. *J. Chem. Phys.* **1997**, *107*, 8110−8119.